

Effects of cooling rate on thermal expansion of $\text{Cu}_{49}\text{Hf}_{42}\text{Al}_9$ metallic glass

WANG Ying-ying, BIAN Xiu-fang, JIA Ran

Key Laboratory of Liquid-Solid Structural Evolution and Processing of Materials of Ministry of Education,
Shandong University, Ji'nan 250061, China

Received 28 September 2010; accepted 31 December 2010

Abstract: Effects of cooling rate on thermal expansion of $\text{Cu}_{49}\text{Hf}_{42}\text{Al}_9$ metallic glass were studied. Five types of amorphous samples with different sizes were prepared in order to get a broad range of cooling rates (from 10^2 to 10^7 K/s). The average thermal expansion coefficients (α_{aver}) of as-quenched samples range from 6.14×10^{-6} to 9.20×10^{-6} K^{-1} . When the temperature is below the glass transformation temperature (T_g), α_{aver} of as-quenched samples has a negative correlation with cooling rate; the values of α_{aver} of annealed and crystallized samples are closed to each other. The results indicate that the amount and motion of free volume play important roles in thermal expansion of metallic glasses.

Key words: metallic glass; thermal expansion; cooling rate

1 Introduction

Metallic glasses (MGs), with fundamental scientific importance and engineering application potential, have attracted world-wide interests. Comparing with crystalline solids, metallic glasses exhibit unique structural characteristics, namely compositional homogeneity and the absence of translational periodicity. Their structural defect was characterized by free volume as proposed by TURNBULL and COHEN [1]. Many studies have shown that free volume dominates the properties of metallic glasses, such as mechanical properties [2–3], viscosity [4] and diffusion [5]. The amount of free volume depends on the preparing technique, such as melt quenching or solid state processing (e.g. cold rolling [6–7]), and the production parameters, such as cooling rate [8] or casting temperature [9]. Moreover, during a thermal treatment the amount of free volume also changes owing to the annihilation or generation of free volume [10]. Among the above factors, the cooling rate plays a particularly prominent role in the formation of metallic glasses [11].

Thermal expansion has scientific and technological significance because it affects the applications of materials in variable thermal processes in macroscopic scale, and is closely related to the binding strength and

stability in atomic scale. Furthermore, figuring out the relation between cooling rate and thermal expansion can deepen our understanding about the effects of free volume in metallic glass. However, little experimental research is focused on this. In this work, the influence of cooling rate on thermal expansion behaviors of $\text{Cu}_{49}\text{Hf}_{42}\text{Al}_9$ metallic glass was reported, which was found to possess high glass forming ability, ductility and toughness [12–13]. This work can help to select and design the coefficient of linear thermal expansion (CTE) by altering cooling rate to make metallic glasses available for ranges of applications.

2 Experimental

$\text{Cu}_{49}\text{Hf}_{42}\text{Al}_9$ ingots were prepared by arc melting under a Ti-gettered argon atmosphere in a water-cooled copper hearth. The alloy ingots were melted five times to ensure compositional homogeneity. Then the alloys were re-melted and cast into samples with different sizes. Rods of 2 mm and 3 mm in diameter were prepared by copper mould suction casting in a purified argon atmosphere in an arc furnace. The molds have internal rod-shaped cavities of approximately 50 mm in length. Ribbons were prepared by melt spinning techniques under pressure of high purity argon (with an over-pressure of 50 kPa), and the thicknesses of ribbons

were 0.02, 0.04 and 0.1 mm, respectively.

The amorphous structures of as-quenched samples were characterized by X-ray diffraction (XRD). Thermal behaviors were examined by differential scanning calorimetry (DSC, Netzsch 404C, aluminum crucibles, constant heating rate 0.33 K/s). Thermal expansion curves were measured by dilatometer (DIL, Netzsch 402C, constant heating rate 0.33 K/s). The samples were 10 mm in length, and the compression load (F) during measurement was 0.245 N. For rods, samples used in dilatometric measurements were cut 10 mm in length from the bottom.

Conventional dilatometer applies a compression load to samples for length measurement, so the experiment for ribbon-shaped samples is difficult to implement. Investigators have tried several methods, such as overlapping the amorphous ribbons into blocks with copper wires [14], coiling the ribbons into rolls [15], developing new apparatus just suitable for ribbons [16]. In this study, we used a simple method to carry out the dilatometric measurements for ribbon-shaped samples. Ribbon was placed between two semicylindrical holders, which were made of copper and slightly shorter (about 0.02 mm) than the ribbon. Only the ribbon contacted with the measuring push poles, so the dilatometer measured the length of the ribbon.

3 Results

3.1 Cooling rates for $\text{Cu}_{49}\text{Hf}_{42}\text{Al}_9$ MG samples

LIN and JOHNSON [17] proposed a method to estimate the cooling rate of metallic glass prepared by quenching molten alloys. The formula is

$$\dot{T} \cong 1000/R^2 \quad (1)$$

where \dot{T} is the cooling rate (K/s), and R is the typical dimension of sample (mm). For example, R is half the thickness for ribbons, and radius for rods. The calculated cooling rates of $\text{Cu}_{49}\text{Hf}_{42}\text{Al}_9$ metallic glassy samples are listed in Table 1. It is shown that the cooling rate in our study has a broad range (from about 10^2 to 10^7 K/s).

3.2 X-ray diffraction patterns

Figure 1 shows the XRD patterns of $\text{Cu}_{49}\text{Hf}_{42}\text{Al}_9$

Table 1 Typical dimension R and cooling rate \dot{T} calculated using formula (1) for five types of $\text{Cu}_{49}\text{Hf}_{42}\text{Al}_9$ MG samples

Sample No.	R/mm	$\dot{T}/(\text{K}\cdot\text{s}^{-1})$
S1	1.50	4.4×10^2
S2	1.00	1.0×10^3
S3	0.05	4.0×10^5
S4	0.02	2.5×10^6
S5	0.01	1.0×10^7

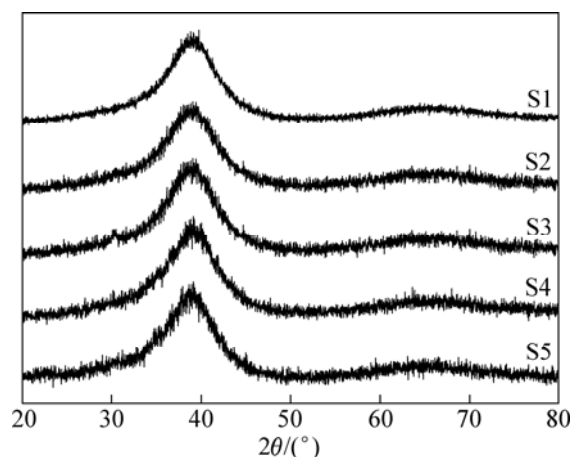


Fig. 1 XRD patterns for $\text{Cu}_{49}\text{Hf}_{42}\text{Al}_9$ metallic glasses

metallic glasses. A characteristic diffuse intensity peak appears from 20° to 50° in the diffraction pattern of each sample, which agrees with the result of Ref. [12].

3.3 DSC analysis

Figure 2 shows the DSC traces of the as-quenched amorphous $\text{Cu}_{49}\text{Hf}_{42}\text{Al}_9$ alloys with the glass transformation temperature T_g and the onset crystallization temperature T_x . For each sample, T_g can be clearly resolved before T_x . The T_g values show a cooling rate dependence: increasing the cooling rate leads to an increase of T_g . Rods have larger temperature interval of supercooled liquid region ΔT_x than ribbons. One main symmetrical crystallization peak is presented on the DSC curve, so rod undergoes eutectic crystallization. Ribbons have more than one crystallization steps, and the pre-peak always occurs clearly separated from the main peak. This is typical for a primary crystallization mechanism. T_g , T_x , and the temperature interval of supercooled liquid region ΔT_x ($\Delta T_x = T_x - T_g$) are listed in Table 2.

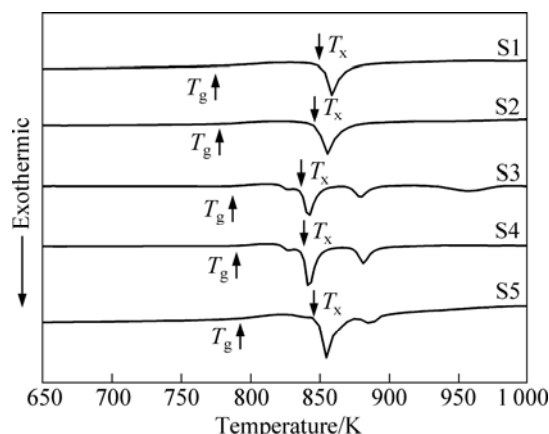
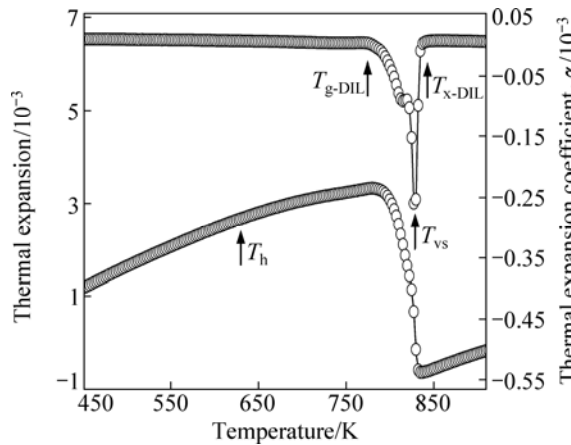


Fig. 2 DSC curves for $\text{Cu}_{49}\text{Hf}_{42}\text{Al}_9$ metallic glasses

Table 2 Glass transformation temperature T_g , onset crystallization temperature T_x , and temperature interval of supercooled liquid region ΔT_x for $\text{Cu}_{49}\text{Hf}_{42}\text{Al}_9$ metallic glasses obtained from DSC curves

Sample No.	T_g/K	T_x/K	$\Delta T_x/\text{K}$
S1	773	850	77
S2	775	846	71
S3	787	834	47
S4	788	837	49
S5	792	845	53

**Fig. 3** Thermal expansion curve and thermal expansion coefficient curves of as-quenched sample S2

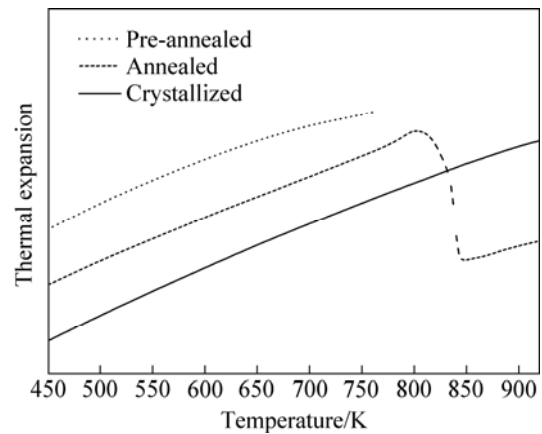
3.4 Thermal expansion behaviors

Figure 3 shows the dilatometric curves of as-quenched sample S2 as an example. Dilatations of as-quenched sample S2 experience three stages: firstly linearly dilating (before T_g), then drastically shrinking (T_g to T_x), and finally linearly dilating again (after T_x). In the linear stage before T_g , the CTE decreases with increasing temperature. The dilatometric curve before T_g can be divided into two steps according to the CTE value. The demarcation point for lower and higher temperature range is marked as T_h . The peak temperature of the thermal expansion coefficient curve is marked as T_{vs} . In Table 3, T_h , T_{g-DIL} , T_{vs} , T_{x-DIL} and ΔT_{x-DIL} obtained from dilatometric measurements are listed.

Table 3 T_h , T_{g-DIL} , T_{vs} , T_{x-DIL} and ΔT_{x-DIL} for as-quenched $\text{Cu}_{49}\text{Hf}_{42}\text{Al}_9$ metallic glasses obtained from dilatometric curves

Sample No.	T_h/K	T_{g-DIL}/K	T_{vs}/K	T_{x-DIL}/K	$\Delta T_{x-DIL}/\text{K}$
S1	580	780	830	866	86
S2	630	775	827	850	75
S3	613	773	823	830	57
S4	616	776	820	836	61
S5	619	775	820	852	77

Dilatation measurements were conducted not only for as-quenched specimens, but also for annealed and crystallized ones. Figure 4 shows the dilatometric curves of sample S2 in different states. In contrast with the as-quenched sample, the annealed one (the ending temperature of pre-annealing is 10 K lower than T_g obtained from DSC curve) keeps a single α_{aver} in the linear dilatation before T_{g-DIL} . The crystallized sample dilates linearly in the whole experimental temperature range. Table 4 lists the α_{aver} values of all the samples in different states. For as-cast sample, α_{aver} decreases with increasing quenching rate. The α_{aver} values of the annealed and crystallized samples are close to each other just as shown in Fig. 4.

**Fig. 4** Thermal expansion curves of sample S2 in different states**Table 4** Average thermal expansion coefficients of $\text{Cu}_{49}\text{Hf}_{42}\text{Al}_9$ metallic glasses in different states

Sample No.	As-quenched (373 K– T_h)		Annealed (373 K– T_g)		Crystallized (373–923 K)	
	$\alpha_{aver}/10^{-6}\text{K}^{-1}$	R^2	$\alpha_{aver}/10^{-6}\text{K}^{-1}$	R^2	$\alpha_{aver}/10^{-6}\text{K}^{-1}$	R^2
S1	9.20	0.999 18	8.54	0.998 88	8.13	0.997 74
S2	8.52	0.997 92	7.51	0.999 36	7.63	0.997 07
S3	6.81	0.997 33	8.46	0.998 94	8.53	0.999 01
S4	6.46	0.997 72	8.64	0.999 05	9.02	0.998 74
S5	6.14	0.992 26	7.80	0.997 51	7.86	0.998 41

4 Discussion

The glass transition characterized by T_g is a kinetic phenomenon which represents the completion of structural relaxation of the glassy material. It is strongly dependent on the thermal history of the sample. When quenched at much higher cooling rate, samples undergo structural relaxation in shorter time scale. Thus, T_g increases with increasing cooling rate as shown in Fig. 2.

Rods have one main symmetrical crystallization peak; while the ribbons have more than one crystallization steps, and the pre-peak always occurs clearly separated from the main peak. Many studies showed that distinct crystallization behaviors of metallic glasses are directly related to and ultimately determined by chemical composition. For instance, SA LISBOA et al [18] proposed a criterion to quantitatively correlate chemical composition with crystallization behaviors of Al-based glass-forming alloys. So we assume that the different crystallization mechanisms of ribbons compared with rods result from the compositional segregation during re-melting in induction furnace.

During the solidification of a supercooled liquid, some excess free volume is frozen in the glassy state. As a result, the dilatation of metallic glasses, unlike crystal alloys, consists of two parts [19]: one is the contribution of the atomic non-harmonic vibration, α_1 (the main source of the dilatation of crystals); and the other is the contribution of free volume motions, α_2 . The effects of cooling rate on the thermal expansion behaviors of $\text{Cu}_{49}\text{Hf}_{42}\text{Al}_9$ metallic glass will be discussed from these two aspects.

Molecular dynamics (MD) research revealed that different cooling rates take no apparent effects on the short-range order of final amorphous state [20]. At a faster cooling rate, the atoms would possess less time to diffuse to a comparatively longer distance, resulting in a looser packed atomic configuration and more quenched-in free volume due to the limited structural relaxation. Such increase in free volume around atoms suggests an enlarged inter-atomic distance, thus decreasing the atomic bonding strength and stability. According to the classical solid theory, the average nearest-neighbor distance (r_0) can be expressed as [21]:

$$r_0 = \left[\frac{(m+n+3)k}{12E\alpha} \right]^{1/3} \quad (2)$$

where E is the elastic modulus; k is the Boltzmann constant; m , n are the constants.

The average nearest-neighbor distance has a negative correlation with the average thermal coefficient

of expansion. Therefore, higher cooling rate leads to lower α_1 .

Excess free volume frozen in the glassy state will be annihilated during annealing at a temperature $T_a < T_g$, or will be generated at an annealing temperature $T_a > T_g$ [22]. When annealing at $T_a < T_g$, the annihilation of free volume causes the sample to contract ($\alpha_2 < 0$). The velocity of annihilation or generation affects α_2 . Samples quenched at faster cooling rate contain more free volume to be annihilated, leading to larger absolute value of α_2 . Consequently, both the dilatation sources (α_1 and α_2) of metallic glass agree with the point well that α_{aver} of the as-quenched metallic glass has a negative correlation with the cooling rate, as shown in Table 4.

In Fig. 3, CTE of as-quenched sample decreases along with temperature before T_g . This is very different from crystal solids, whose CTE generally increases with temperature owing to the increase of vacancies [23]. The reduction of CTE is attributed to the faster annihilation of the free volume in the higher temperature range. In other words, below T_h the free volume is annihilated so slowly that α_2 has little influence on α .

When $\text{Cu}_{49}\text{Hf}_{42}\text{Al}_9$ metallic glass is heated to a temperature (T_a) which is higher than T_g , a large number of free volume is generated, causing the sample to dilate ($\alpha_2 > 0$). As a result, α increases substantially [24]. However, as shown in Fig. 3, the dilatation curves of as-quenched samples decrease drastically within the supercooled liquid state. This is due to the viscous flow under the action of the compression load [25].

Although this segment of the curve could not reflect the true dilatometric behavior of the as-quenched sample, the viscous flow behavior of the $\text{Cu}_{49}\text{Hf}_{42}\text{Al}_9$ metallic glass in the supercooled viscous region could help to search the optimum superplastic forming condition [26]. The appropriate working temperature for microforming can be determined by the steady state viscous flow temperature T_{vs} . The differentia between the viscous flow temperatures of samples is not only caused by the structural differences, which has been confirmed by XRD and DSC experiments, but also by the different stress applied on the samples.

After structural relaxation in pre-annealing process, most excess free volume has been annihilated. The contribution of free volume motions becomes neglectable for the amount of free volume in the annealed sample is lower and steady. Thus, the thermal expansion curve of the annealed sample is a straight line below T_g as shown in Fig. 4.

The crystallized sample dilates linearly in the whole experimental temperature range, indicating that no phase transformation exists. Since dilation of both the annealed

and crystallized samples is mainly sourced from the atomic non-harmonic vibration, they show similar α_{aver} in the linear expansion segment.

5 Conclusions

1) Thermal expansion curves distinctly reveal the glass transition temperature (T_g), the crystallization temperature (T_x) and the optimum temperature (T_{vs}) for superplastic forming.

2) For $\text{Cu}_{49}\text{Hf}_{42}\text{Al}_9$ metallic glass, below T_g , the annealed and crystallized samples show similar average thermal expansion coefficient.

3) The average thermal expansion coefficient (α_{aver}) of as-quenched $\text{Cu}_{49}\text{Hf}_{42}\text{Al}_9$ metallic glass samples has a negative correlation with cooling rate when the temperature is below T_g . When the cooling rate increases from 10^2 to 10^7 K/s, α_{aver} descends from 9.20×10^{-6} to 6.14×10^{-6} K^{-1} . Hence, in order to obtain smaller dilatation of metallic glass in thermal process, lower cooling rate should be utilized.

References

- TURNBULL D, COHEN M H. Free-volume model of the amorphous phase: Glass transition [J]. *The Journal of Chemical Physics*, 1961, 34: 120–125.
- LAUNEY M E, KRUZIC J J, LI C, BUSCH R. Quantification of free volume differences in a $\text{Zr}_{44}\text{Ti}_{11}\text{Ni}_{10}\text{Cu}_{10}\text{Be}_{25}$ bulk amorphous alloy [J]. *Applied Physics Letters*, 2007, 91: 051913.
- LIU Hui-bin, LI Jin-fu, CAO Qing-ping, ZHOU Yao-he. Free-volume evolution of glassy $\text{Zr}_{65}\text{Al}_{7.5}\text{Ni}_{10}\text{Cu}_{17.5}$ during inhomogeneous deformation [J]. *Chinese Science Bulletin*, 2007, 52(24): 3443–3447.
- MUKHERJE S, SCHROERS J, ZHOU Z, JOHNSON W L, RHIM W K. Viscosity and specific volume of bulk metallic glass-forming alloys and their correlation with glass forming ability [J]. *Acta Materialia*, 2004, 52: 3689–3695.
- FAUPEL F, FRANK W, MACHT M P, MEHRER H, NAUNDORF V, RATZKE K, SCHOBER H R, SHARMA S K, TEICHLER H. Diffusion in metallic glasses and supercooled melts [J]. *Reviews of Modern Physics*, 2003, 75: 237–280.
- CAO Q P, LI J F, ZHOU Y H, HORSEWELL A, JIANG J Z. Free volume evolution and its temperature dependence during rolling of $\text{Cu}_{60}\text{Zr}_{20}\text{Ti}_{20}$ bulk metallic glass [J]. *Applied Physics Letters*, 2005, 87(10): 101901.
- JIANG W H, PINKERTON F E, ATZMON M. Mechanical behavior of shear bands and the effect of their relaxation in a rolled amorphous Al-based alloy [J]. *Acta Materialia*, 2005, 53: 3469–3477.
- LIU Y, BEI H, LIU C T, GEORGE E P. Cooling-rate induced softening in a $\text{Zr}_{50}\text{Cu}_{50}$ bulk metallic glass [J]. *Applied Physics Letters*, 2007, 90: 071909.
- MAO J, ZHANG H F, FU H M, WANG A M, LIA H, HU Z Q. Effects of casting temperature on mechanical properties of Zr-based metallic glasses [J]. *Materials Science and Engineering A*, 2010, 527: 981–985.
- SLIPENYUK A, EEKERT J. Correlation between enthalpy change and free volume reduction during structural relaxation of $\text{Zr}_{55}\text{Cu}_{30}\text{Al}_{10}\text{Ni}_5$ metallic glass [J]. *Scripta Materialia*, 2004, 50: 39–44.
- HENG Cai-xing, LIU Rang-su, PENG Ping. Molecular dynamics simulation of amorphous formation during solidification processes of liquid metal Ag_6Cu_4 [J]. *The Chinese Journal of Nonferrous Metals*, 2003, 13(6): 1333–1337. (in Chinese)
- JIA P, GUO H, LI Y, XU J, MA E. A new Cu-Hf-Al ternary bulk metallic glass with high glass forming ability and ductility [J]. *Scripta Materialia*, 2006, 54: 2165–2168.
- JIA P, ZHU Z D, MA E, XU J. Notch toughness of Cu-based bulk metallic glasses [J]. *Scripta Materialia*, 2009, 61: 137–140.
- LI G H, WANG W M, BIAN X F, ZHANG J T, LIA R, QIN J Y. Correlation between thermal expansion coefficient and glass formability in amorphous alloys [J]. *Materials Chemistry and Physics*, 2009, 116: 72–75.
- NIU Y C, BIAN X F, WANG W M, JIN S F, LIU X J, ZHANG J Y, QIN G L [J]. *Journal of Non-Crystalline Solids*, 2005, 351: 3854–3860.
- VLASAK G, DUHAJ P, PATRASOVA H, SVEC P. Apparatus for thermal dilatation and magnetostriction measurements of amorphous ribbons [J]. *Journal of Physics E: Scientific Instruments*, 1983, 16: 1203–1207.
- LIN X H, JOHNSON W L. Formation of Ti-Zr-Cu-Ni bulk metallic glasses [J]. *Journal of Applied Physics*, 1995, 78: 6514–6519.
- SA LISBOA R D, BOLFARINI C, BOTTA F W J, KIMINAMI C S. Topological instability as a criterion for design and selection of aluminum-based glass-former alloys [J]. *Applied Physics Letters*, 2005, 86: 211904.
- YAVARI A R, MOULEC A L, INOUE A, NISHIYAMA N, LUPU N, MATSUBARA E, BOTTA W J, VAUGHAN G, MICHEL M D, KVICK A. Excess free volume in metallic glasses measured by X-ray diffraction [J]. *Acta Materialia*, 2005, 53: 1611–1619.
- WANG J T, HODGSONA P D, ZHANG J D, YAN W Y, YANG C H. Effects of quenching rate on amorphous structures of $\text{Cu}_{46}\text{Zr}_{54}$ metallic glass [J]. *Journal of Materials Processing Technology*, 2009, 209: 4601–4606.
- PORSCHA B, NEUHAUSER H. Combined measurements of length and modulus change and calculation of effective pair potentials for the amorphous alloy $\text{Cu}_{64}\text{Ti}_{36}$ [J]. *Physica Status Solidi B*, 1994, 186: 119–126.
- RUSSEW K, STOJANOVA L, SOMMER F. Viscous flow, thermal expansion and heat capacity of $\text{Fe}_{25}\text{Zr}_{75}$ glassy alloy under non-isothermal conditions at different heating rates [J]. *Materials Science and Engineering A*, 1997, 226–228: 344–347.
- ZUBOV V I, ZUBOV I V. Thermal vacancy effects on the thermodynamic properties and stability of fullerites [J]. *Journal of Physical Chemistry B*, 2005, 109: 14627–14631.
- LU I R, GORLER G P, WILLNECKER R. Specific volume of glass-forming liquid $\text{Pd}_{43}\text{Cu}_{27}\text{Ni}_{10}\text{P}_{20}$ and related thermodynamic aspects of the glass transition [J]. *Applied Physics Letters*, 2002, 80: 4534–4536.
- SCHERMAYER D, NEUHAUSER H. Dilatometric measurements on metallic glass ribbons with a wide glass transition range [J]. *Materials Science and Engineering A*, 1997, 226–228: 846–850.
- CHANG Y C, HUNG T H, CHEN H M, HUANG J C, NIEH T G, LEE C J. Viscous flow behavior and thermal properties of bulk amorphous $\text{Mg}_{58}\text{Cu}_{31}\text{Y}_{11}$ alloy [J]. *Intermetallics*, 2007, 15: 1303–1308.

冷却速率对 $\text{Cu}_{49}\text{Hf}_{42}\text{Al}_9$ 金属玻璃热膨胀的影响

王莹莹, 边秀房, 贾然

山东大学 材料液固结构演变与加工教育部重点实验室, 济南 250061

摘要: 研究冷却速率对 $\text{Cu}_{49}\text{Hf}_{42}\text{Al}_9$ 金属玻璃热膨胀行为的影响。为了得到较大范围的冷却速率, 制备了 5 种不同尺寸的非晶样品(冷却速率范围为 $10^2\sim 10^7$ K/s)。淬火态样品的平均热膨胀系数(α_{aver})分布于 6.14×10^{-6} K^{-1} 至 9.20×10^{-6} K^{-1} 之间。在玻璃转变温度(T_g)以下时, 淬火态样品的平均热膨胀系数(α_{aver})与冷却速率呈反比; 退火态与晶态样品具有相似的平均热膨胀系数。结果表明, 自由体积的数量和运动对于金属玻璃的热膨胀具有重要作用。

关键词: 金属玻璃; 热膨胀; 冷却速率

(Edited by LI Xiang-qun)